Journal of Hydroscience and Hydraulic Engineering
Vol. 18, No.1 May, 2000, 85-95

NUMERICAL MODEL FOR 2-D TRANSIENT FREE SURFACE FLOWS WITH OBSTRUCTIONS

By

Juichiro Akiyama, Masaru Ura, Mirei Shigeeda and Yoshitaka Arita

Department of Civil Engineering, Kyushu Institute of Technology, Kitakyushu 804-8550, Japan

SYNOPSIS

A second-order accurate numerical model for two-dimensional flood flow is developed based on high-resolution TVD-MacCormack scheme. The cell-averaged flow variables are used to include the effects of obstructions within a cell on the flow in the model. The drag force is modeled with drag coefficient and the ratio of obstructions' area to the cell area. The performance of the model is verified against the Stoker's analytical solution for a one-dimensional dam-break problem and the experimental data on one- and two-dimensional dam-break flood waves propagating in a horizontal channel where equi-spaced cylinders are placed over the full and half width of the channel. Sensitivity analysis related to the effects of obstructions on the flow is also performed.

INTRODUCTION

River basins are almost always concentrated with population and property. Areas in the vicinity of rivers are also most likely to be flooded following heavy rainfall in these areas or in the catchments upstream. Flooding in the densely populated and well developed areas may be characterized by flood flows obstructed and often guided by such obstructions as buildings, posts, trees etc. A numerical model for simulation of such flood flows must take into account these obstructions as well as other relevant flood phenomenon.

A flood simulation model generally consists of a numerical model for two-dimensional flood flow based on shallow water equations and techniques to treat arbitrary flood-plain geometry and topography with road networks, buildings, vegetation, structures, and others. There exist many flood simulation models ((1), (2), (3), and (4)). Iwasa et al. (1) developed a flood simulation model for a flood-plain with drainage channels and embankments. Takahashi and Nakagawa (2) made some modifications, and applied it to urban areas. This model is based on a very diffusive scheme. Suetugi and Kuriki (3) proposed a flood simulation model with land-uses dependent roughness coefficients and applied it to the Chikugo and the Turumi river basins. However the basis of the artificial viscosity used in the model is uncertain. Fukuoka et al. (4) constructed a flood simulation model for urban residential areas. The model makes use of the general curvilinear coordinates applied to arbitrary geometry consisting of road networks and houses. The hydrodynamic force acting on the obstructions was estimated from the depths, both in front and at back sides of an obstruction. The model was verified by comparing the experimental data conducted under simplified situation of the real urban residential areas. However, the scheme used in the model is not explained in detail.

High resolution schemes such as FDS, MUSCL, etc. have been proposed for the Euler equations in the field of computational fluid dynamics(CFD)(5). Similar to the Euler equations, the shallow water equations are hyperbolic. With suitable modifications, high-resolution schemes developed for the Euler equations can be utilized to develop a flood simulation model with higher accuracy than existing ones (e.g. (6) and (7)). Glaister (8), Alcrudo et al. (9), Fraccarollo and Toro (10) and Zhao et al. (11), for instance, have demonstrated such a possibility.

This work is a first step in construction of an accurate flood simulation model. A second-order accurate numerical model for two-dimensional flood flow based on the shallow water equations is developed. In this model, a technique to treat obstructions, which correspond to trees, buildings, and others, within a cell is considered, and the cell-averaged flow variables are used in a manner similar to Raupach

and Shaw (12). The drag force on the obstructions is modeled with both drag coefficient and ratio of obstructions area to cell area. The TVD-MacCormack scheme is employed as a high-resolution scheme. The scheme consists of MacCormack scheme and a TVD term. A TVD term adds dissipation, according to the theory of TVD, to MacCormack scheme and provides oscillation free solutions. The performance of the model is verified against the Stoker's analytical solution for a one-dimensional dam-break problem and the experimental data on one- and two-dimensional dam-break flood waves propagating in a horizontal channel with equi-spaced cylinders, which are not submerged, placed over the full and half width of the channel. Additionally, sensitivity analysis for both the drag coefficient and area ratio in the drag force are performed.

GOVERNING EQUATIONS

The governing equations for two-dimensional unsteady free surface flows can be written as

$$\frac{\partial \boldsymbol{U}}{\partial t} + \frac{\partial \boldsymbol{E}}{\partial x} + \frac{\partial \boldsymbol{F}}{\partial y} + \boldsymbol{S}_x + \boldsymbol{S}_y = \boldsymbol{0} \tag{1}$$

where $\boldsymbol{U}$ = vector of unknowns; $\boldsymbol{E}$ and $\boldsymbol{F}$ = components of the flux along x- and y-directions, respectively; $\boldsymbol{S}_x$ and $\boldsymbol{S}_y$ = vectors containing source and sink terms along x- and y-directions, respectively.

These vectors are given by

$$\begin{aligned} &\boldsymbol{U} = (h, uh, vh)^T\,;\ \boldsymbol{E} = \left(uh, u^2h + \frac{1}{2}gh^2, uvh\right)^T\,;\ \boldsymbol{F} = \left(vh, uvh, v^2h + \frac{1}{2}gh^2\right)^T \\ &\boldsymbol{S}_x = (0, -gh\,(S_{ox} - S_{fx}) + F_x, 0)^T\,;\ \boldsymbol{S}_y = (0, 0, -gh\,(S_{oy} - S_{fy}) + F_y)^T \end{aligned} \tag{2}$$

where h = water depth; u and v = velocity components along x and y directions, respectively; g = acceleration due to gravity; S_{ox} and S_{oy} = bed-slopes along x and y directions, respectively; S_{fx} and S_{fy} = friction slopes along x and y directions, respectively; F_x and F_y = components of the drag forces due to obstructions within a cell along x and y directions, respectively.

The bed slopes S_{ox} and S_{oy} are defined respectively as

$$S_{ox} = -\frac{\partial z_b}{\partial x};\quad S_{oy} = -\frac{\partial z_b}{\partial y} \tag{3}$$

where z_b = bed elevation abqve a reference datum.

The friction slopes S_{fx} and S_{fy} are assumed to be given by Manning's formula. Thus,

$$S_{fx} = \frac{n^2 u\sqrt{u^2+v^2}}{h^{4/3}};\quad S_{fy} = \frac{n^2 v\sqrt{u^2+v^2}}{h^{4/3}} \tag{4}$$

where n = Manning's roughness coefficient.

The effect of the obstructions within a cell on the flow is modeled as a drag force term. The drag forces F_x and F_y are defined as

$$F_x = \frac{1}{2}\lambda C_d uh\sqrt{u^2+v^2};\quad F_y = \frac{1}{2}\lambda C_d vh\sqrt{u^2+v^2} \tag{5}$$

where C_d = drag coefficient; and λ = the ratio of obstructions area to cell area termed as area ratio.

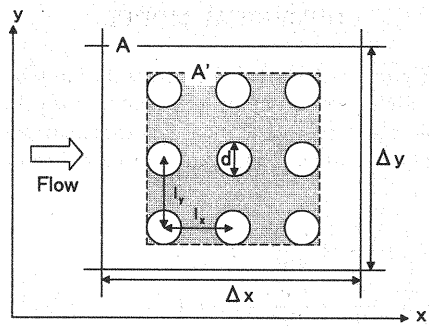

Fig.1 Definition of symbols used for area ratio λ.

$$\lambda = \frac{\lambda' A'}{A} \tag{6}$$

where A = cell area; A' = area within a cell circumscribing obstructions; λ' = density of obstructions in a cell for the obstructions arrangements considered here (13)(see Fig.1).

$$\lambda' = \frac{d}{a I_x I_y} \tag{7}$$

where d = projected width of obstructions against main flow; I_x and I_y = obstructions' spacing along x, y direction, respectively; a = coefficient of obstructions' pattern. $a = 1$ for parallel pattern and $a = 2$ for staggered pattern.

$\boldsymbol{E}$ and $\boldsymbol{F}$ have their Jacobian vectors $\boldsymbol{A}$ and $\boldsymbol{B}$, respectively, with respect to $\boldsymbol{U}$, which are given by

$$\boldsymbol{A} = \frac{\partial \boldsymbol{E}}{\partial \boldsymbol{U}} = \begin{pmatrix} 0 & 1 & 0 \\ -u^2 + c^2 & 2u & 0 \\ -uv & v & u \end{pmatrix} ; \boldsymbol{B} = \frac{\partial \boldsymbol{F}}{\partial \boldsymbol{U}} = \begin{pmatrix} 0 & 0 & 1 \\ -uv & v & u \\ -v^2 + c^2 & 0 & 2v \end{pmatrix} \tag{8}$$

where c = the wave speed($= \sqrt{gh}$).
The eigenvalues and eigenvectors of $\boldsymbol{A}$ are

$$\lambda^1 = u, \lambda^2 = u + c, \lambda^3 = u - c \tag{9}$$

$$\boldsymbol{e}^1 = \begin{pmatrix} 0 & 0 & 1 \end{pmatrix}^T ; \boldsymbol{e}^2 = \begin{pmatrix} 1 & u+c & v \end{pmatrix}^T ; \boldsymbol{e}^3 = \begin{pmatrix} 1 & u-c & v \end{pmatrix}^T \tag{10}$$

The eigenvalues and eigenvectors of $\boldsymbol{B}$ are

$$\omega^1 = v, \omega^2 = v + c, \omega^3 = v - c \tag{11}$$

$$\boldsymbol{f}^1 = \begin{pmatrix} 0 & 1 & 0 \end{pmatrix}^T ; \boldsymbol{f}^2 = \begin{pmatrix} 1 & u & v+c \end{pmatrix}^T ; \boldsymbol{f}^3 = \begin{pmatrix} 1 & u & v-c \end{pmatrix}^T \tag{12}$$

The eigenvalues of $\boldsymbol{A}$ and $\boldsymbol{B}$ are the characteristic speeds and their signs provide the information about the direction of propagation of the flow.

NUMERICAL MODEL

The TVD-MacCormack scheme is adopted as a high resolution scheme because of easy incorporation of source terms while maintaining second-order accuracy in both time and space.

The two-dimensional problem is decomposed into the problem of solving a pair of one-dimensional problems using operator splitting technique. Thus, Eq.1 can be written as

$$\frac{\partial \boldsymbol{U}}{\partial t} + \frac{\partial \boldsymbol{E}}{\partial x} + \boldsymbol{S}_x = \boldsymbol{0} \tag{13a}$$

$$\frac{\partial \boldsymbol{U}}{\partial t} + \frac{\partial \boldsymbol{F}}{\partial y} + \boldsymbol{S}_y = \boldsymbol{0} \tag{13b}$$

Operator splitting used in this work is as follows:

$$\boldsymbol{U}_{i,j}^{t+1} = L_x\left(\frac{\Delta t}{2}\right) L_y\left(\frac{\Delta t}{2}\right) L_y\left(\frac{\Delta t}{2}\right) L_x\left(\frac{\Delta t}{2}\right) \boldsymbol{U}_{i,j}^{t} \tag{14}$$

where L = integration in time, the quantity in the bracket denotes time increment, and the subscripts, x and y, denote the direction of computation. The solution along x-direction is described in the following. MacCormack's two-step predictor and corrector scheme for Eq.13a can be written as

Predictor Step:

$$\boldsymbol{U}_{i,j}^{p} = \boldsymbol{U}_{i,j}^{t} - \frac{\Delta t}{\Delta x}\left\{(1-\theta_x)\,\boldsymbol{E}_{i+1,j}^{t} - (1-2\theta_x)\,\boldsymbol{E}_{i,j}^{t} - \theta_x \boldsymbol{E}_{i-1,j}^{t}\right\} - \Delta t \boldsymbol{S}_{x\,i,j}^{t} \tag{15}$$

Corrector Step:

$$\boldsymbol{U}_{i,j}^{c} = \boldsymbol{U}_{i,j}^{p} - \frac{\Delta t}{\Delta x}\left\{(1-\theta_x)\,\boldsymbol{E}_{i+1,j}^{p} - (1-2\theta_x)\,\boldsymbol{E}_{i,j}^{p} - \theta_x \boldsymbol{E}_{i-1,j}^{p}\right\} - \Delta t \boldsymbol{S}_{x\,i,j}^{p} \tag{16}$$

The updated variables at the new time level $t+1$ are then obtained as

$$\boldsymbol{U}_{i,j}^{'t+1} = \frac{1}{2}\left(\boldsymbol{U}_{i,j}^{t} + \boldsymbol{U}_{i,j}^{c}\right) \tag{17}$$

where Δt = time step; Δx = grid size along x-direction. The superscripts, p and c, stand for predicted and corrected variables, respectively; θ_x = parameter determining the direction of space difference for removing most of the directional bias (14). The corrected variables obtained by Eq.17 are modified with a TVD term as

$$\boldsymbol{U}_{i,j}^{t+1} = \boldsymbol{U}_{i,j}^{'t+1} + \boldsymbol{G}_{x\,i+1/2,j} - \boldsymbol{G}_{x\,i-1/2,j} \tag{18}$$

where $\boldsymbol{G}$ = upwind TVD term. Addition of the TVD term to MacCormack scheme gives TVD property for an oscillation free solution, while retaining second-order accuracy in space and time to the scheme. The TVD term allows solution of sub- and supercritical flows with high accuracy and can be written as

$$G_{x\,i+1/2,j} = \frac{1}{2}\frac{\Delta t}{\Delta x}\sum_{k=1}^{3}\left[\alpha^k_{i+1/2,j}\Psi\left(\tilde{\lambda}^k_{i+1/2,j}\right)\right.$$
$$\left. - \alpha^k_{i+1/2,j}\left|\tilde{\lambda}^k_{i+1/2,j}\right|\left(\frac{\Delta t}{\Delta x}\left|\tilde{\lambda}^k_{i+1/2,j}\right|\right)\right]\left[1-\phi\left(r^k_{x\,i+1/2,j}\right)\right]\tilde{e}^k_{i+1/2,j} \quad (19)$$

where $\tilde{\lambda}$ and $\tilde{e}$ are eigenvalues and eigenvectors, respectively, evaluated by Roe's average defined by

$$\tilde{u}_{i+1/2,j} = \frac{\sqrt{h_{i+1,j}}u_{i+1,j} + \sqrt{h_{i,j}}u_{i,j}}{\sqrt{h_{i+1,j}} + \sqrt{h_{i,j}}}$$
$$\tilde{v}_{i+1/2,j} = \frac{\sqrt{h_{i+1,j}}v_{i+1,j} + \sqrt{h_{i,j}}v_{i,j}}{\sqrt{h_{i+1,j}} + \sqrt{h_{i,j}}} \quad (20)$$
$$\tilde{c}_{i+1/2,j} = \sqrt{\frac{g\left(h_{i+1,j}+h_{i.j}\right)}{2}}$$

The α in Eq.19 are wave strengths expressed as

$$\alpha^1_{i+1/2,j} = -\tilde{v}_{i+1/2,j}\left(h_{i+1,j}-h_{i,j}\right) + \left(v_{i+1,j}h_{i+1,j} - v_{i,j}h_{i,j}\right)$$
$$\alpha^2_{i+1/2,j} = -\frac{1}{2\tilde{c}_{i+1/2,j}}\left\{\left(\tilde{u}_{i+1/2,j}-\tilde{c}_{i+1/2,j}\right)\left(h_{i+1,j}-h_{i,j}\right) - \left(u_{i+1,j}h_{i+1,j} - u_{i,j}h_{i,j}\right)\right\} \quad (21)$$
$$\alpha^3_{i+1/2,j} = \frac{1}{2\tilde{c}_{i+1/2,j}}\left\{\left(\tilde{u}_{i+1/2,j}+\tilde{c}_{i+1/2,j}\right)\left(h_{i+1,j}-h_{i,j}\right) - \left(u_{i+1,j}h_{i+1,j} - u_{i,j}h_{i,j}\right)\right\}$$

where the function Ψ in Eq.19 is an entropy correction to $\tilde{\alpha}$ (15).

$$\psi\left(\tilde{\lambda}^k_{i\pm1/2,j}\right) = \max\left(\delta_{i\pm1/2,j}, \left|\tilde{\lambda}^k_{i\pm1/2,j}\right|\right)$$
$$\delta_{i+1/2,j} = \max\left(\ 0,\quad \lambda\left(U_{i,j}\,,U_{i+1,j}\right) - \lambda\left(U_{i,j}\right),\ \lambda\left(U_{i+1,j}\right) - \lambda\left(U_{i,j}\,,U_{i+1,j}\right)\ \right) \quad (22)$$
$$\delta_{i-1/2,j} = \max\left(\ 0,\quad \lambda\left(U_{i-1,j}\,,U_{i,j}\right) - \lambda\left(U_{i-1,j}\right),\ \lambda\left(U_{i,j}\right) - \lambda\left(U_{i-1,j}\,,U_{i,j}\right)\ \right)$$

The factor ϕ in Eq.19 is a limiter, which guarantees second order accuracy while preventing oscillation. The limiter is a non-linear function of

$$r^k_{x\,i+1/2,j} = \frac{\alpha^k_{i+1/2-s_x,j}}{\alpha^k_{i+1/2,j}},\ s_x = sgn\left(\lambda^k_{i+1/2,\,j}\right) \quad (23)$$

We use Van Leer limiter (16) expressed as

$$\phi\left(r\right) = \frac{|r|+r}{1+|r|} \quad (24)$$

MODEL VERIFICATION

Dam break problem

The validity of the model is examined by comparing the computed results with the Stoker's analytical solution (17) for a dam-break problem. The dam-break problem is illustrated in Fig.2. The

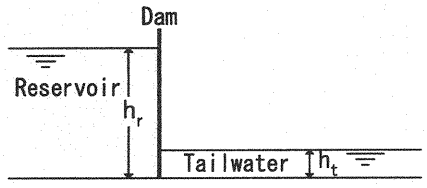

Fig.2 Dam-break problem.

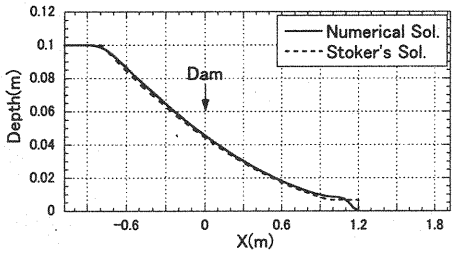

(a) depth

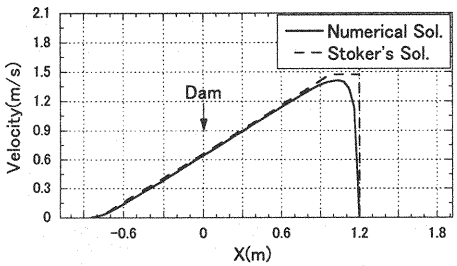

(b) velocity

Fig.3 Comparison with analytical solutions.

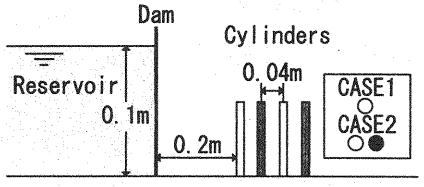

(a) side view

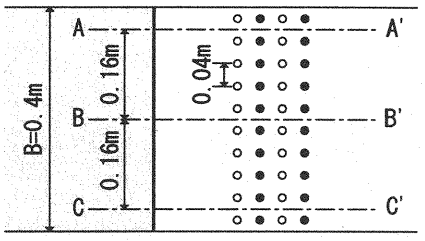

(b) plane view

Fig.4 Arrangements of cylinders.

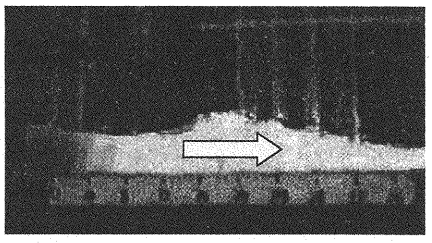

Fig.5 Flow profile.

channel is 3.20m long with a dam placed at 1.08m from the upstream end of the channel. Initially the reservoir depth h_r is 0.1m and the tailwater depth h_t is 0.0001m, i.e. the depth ratio h_t/h_r equals to 0.001. The grid size (Δx) is 0.04m and the Courant number C_r is set to 0.8. The computed results at 0.8 seconds are compared with the analytical solutions in Fig.3. The calculated result matches with the analytical solution, with only slight difference in the front resolution.

Dam-break problem with solid cylinders

The experiments were conducted in a rectangular channel 3.2m long and 0.4m wide with cylinders placed at 0.2m downstream of the dam, which itself was placed at 1.08m from the upstream end of the channel. The cylinder is made of Perspex and its diameter is 0.01m. The arrangements of cylinders is shown in Fig.4. Three cases of experiments were conducted, changing the arrangements of cylinders; Case1 had two parallel rows of equi-spaced solid cylinders across the full width of the channel; Case2 had four such rows; Case3 had four rows of equi-spaced solid cylinders across the half of the channel width. In all cases the initial reservoir depth was set to 0.1m and the tailwater depth was 0.0m, i.e. dry-bed condition.

A dam-break flow was produced by instantaneously opening a gate, which modeled the dam. The flow was visualized using a laser light sheet and was recorded with a VTR. The time required to open the gate was about 0.025 seconds. A water surface profile along B-B' (see Fig.4) at a given time was obtained by analyzing the recorded images with computer. Each experiment was repeated five times under the same condition in order to obtain accurate data. Fig.5 shows an example of the flow at t = 1.3 seconds.

The computational grid size ($\Delta x \times \Delta y$) is 0.04m × 0.04m and the Courant number used is the

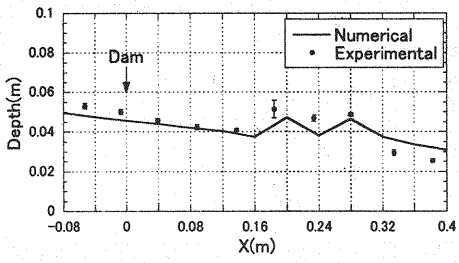

(a) 0.9 seconds

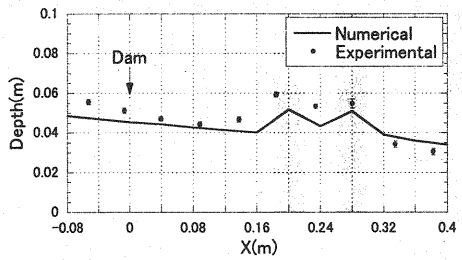

(b) 1.1 seconds

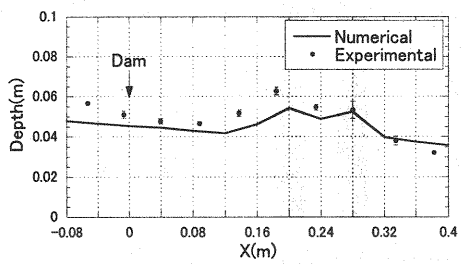

(c) 1.3 seconds

Fig.6 Comparison with the experiment Case1.

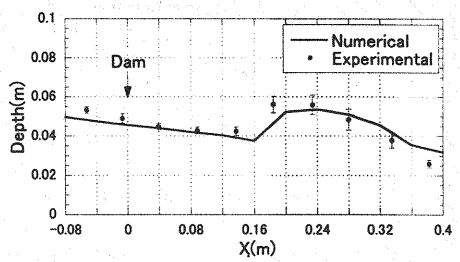

(a) 0.9 seconds

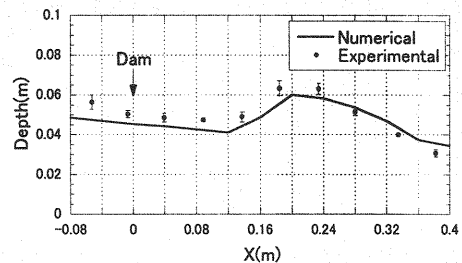

(b) 1.1 seconds

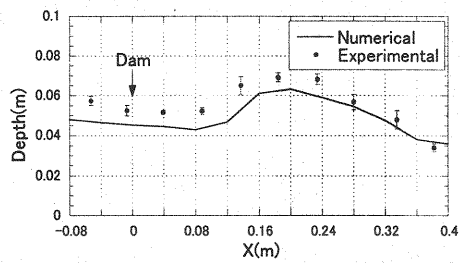

(c) 1.3 seconds

Fig.7 Comparison with the experiment Case2.

same as before. The drag coefficient of 1.2 is used. Although the experiments were conducted with dry-bed condition, the model works only when $h_t/h_r \geq 0.001$, and hence h_t is set to be 0.0001m.

Fig.6 and Fig.7 are examples of comparisons between computed results and experimental data for Case1 and Case2, respectively. In the figures the shadow indicates the region wherein cylinders are placed. The symbol • and the error-bar represent the mean values of experimental data and the standard deviation of experimental data, respectively. These figures show that the standard deviation is small, indicating that the reproduction of the experiments is satisfactory. No difference between the water surface profiles at the center and near the side walls of the channel is observed. The agreement between computed and experimental results is satisfactory. However, in the upstream of cylinders and in the domain where cylinders exist the computed values are a little lower than the experimental ones, while the reverse is true in the downstream of cylinders. These differences may be due to such reasons as; use of the steady state value of drag coefficient($C_d = 1.2$), no consideration of the source term in the TVD term, non dry-bed conditions in the computation. In addition, water splashes when the flow hits the cylinders and delay in gate openings may also cause the difference.

Fig.8 compares computed results with experimental data for Case3. In this case we compare water surface profiles along A-A', B-B', and C-C'(see Fig.4). The symbols in Fig.8 are the same as in Case1 and Case2. Even in Case3 only small standard deviation is observed, and hence the reproduction of the experimental results is satisfactory. The agreement between the computed and experimental results is satisfactory along every cross section. In the upstream of cylinders, however, computed values are a little lower than the experimental ones, while the reverse is seen in the downstream of the cylinders. The reasons for this difference are believed to be the same as in Case1 and Case2.

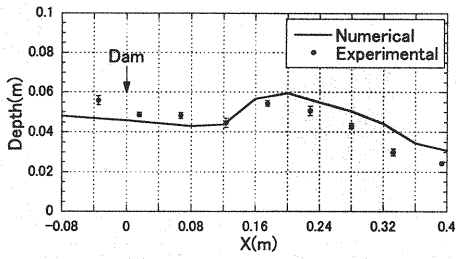

(a) A-A'

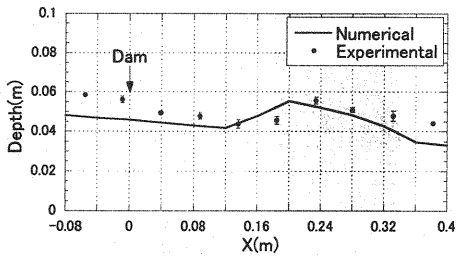

(b) B-B'

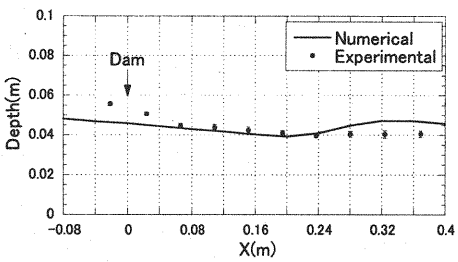

(c) C-C'

Fig.8 Comparison with the experiment Case3.

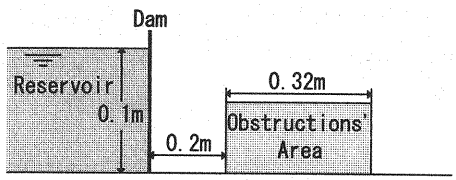

(a) side view

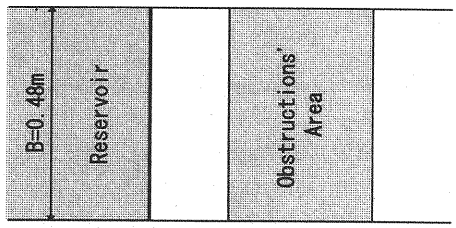

(b) plane view

Fig.9 Numerical experiment condition.

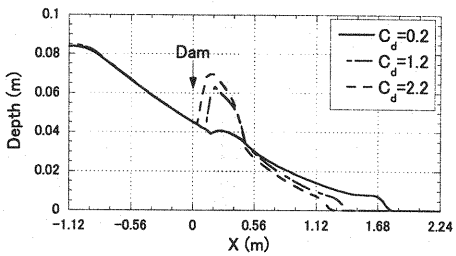

Fig.10 Effect of the drag coefficient.

SENSITIVITY ANALYSIS

To investigate the effects of obstructions' shapes and arrangement patterns on the dam-break flow and the effects of the grid size on computation of obstructions, different values of the drag coefficients, the area ratios and the grid sizes are tested.

Effect of the drag coefficient

Three drag coefficients, C_d=0.2, 1.2, and 2.2 are used to examine the effects of the drag coefficient on the dam-break flow under the presence of obstructions. The channel is horizontal, frictionless and rectangular (3.36m long and 0.48m wide) with obstructions placed downstream of 0.2m from the dam. The dam was placed at 1.12m from upstream end of the channel(see Fig.9). The depth upstream of the dam, the tail water depth, the grid size, and the Courant number are the same as before.

The simulated water surface profiles, at 1.3 seconds after sudden dam removal, are shown in Fig.10. The results indicate that the wave front is retarded and the depth in the downstream of the dam increases as the drag coefficient is increased. The model response to the variations in drag coefficient seems reasonable.

Effect of the area ratio

The effects of area ratio on the flow are examined by changing arrangement patterns of obstructions, values of a projected width of obstruction, and obstructions' spacing. In all cases C_d = 1.2 is

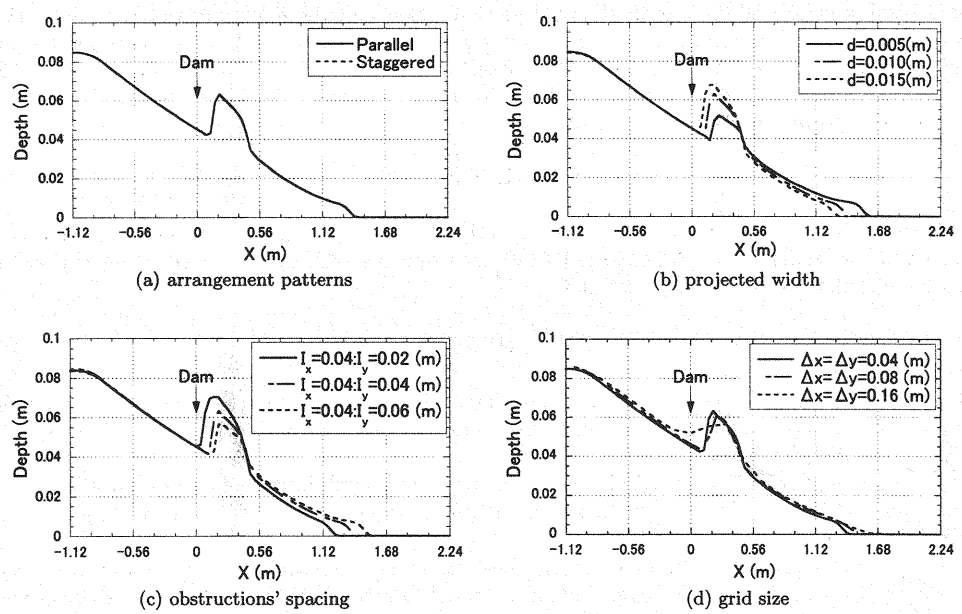

(a) arrangement patterns (b) projected width

(c) obstructions' spacing (d) grid size

Fig.11 Effect of the area ratio and the grid size.

used.

The effect of arrangement patterns of obstructions on the flow is investigated through two patterns, parallel($I_x = I_y = 0.04$m) and staggered($I_x = 0.04$m, $I_y = 0.02$m). The water surface profiles at 1.3 seconds are shown in Fig.11(a). As obvious from model formulation(Eq.7), the area ratio for the two patterns are equal. So the same results are obtained.

In the case to investigate the effect of a projected width and obstruction spacings, three projected widths of 0.005m, 0.01m, and 0.015m and obstruction spacings($I_x \times I_y$) of 0.04m×0.02m, 0.04m×0.04m, and 0.04m×0.06m are adopted.The arrangement pattern used is parallel. The water surface profiles at 1.3 seconds are shown in Fig.11(b) and Fig.11(c). The results indicate that the wave front moves slower as the projected width increases or as the spacing decreases, and the depth immediately downstream of the dam becomes higher as the projected width increases or as the obstruction spacing decreases. The model response to the area ratio seems reasonable.

Effect of the grid size on computation of obstructions

As the grid size is increased, the effect of even the localized obstructions must spread over the whole mesh. Therefore, the rise in water level due to obstructions appear diffused in space. The reverse is true when the grid size becomes finer.

For investigating the effect of the grid size on computation of obstructions, three grid size of 0.04m × 0.04m, 0.08m × 0.08m, and 0.16m × 0.16m are adopted. The obstructions' arrangement pattern is parallel, the projected width is 0.01m, and the obstructions' spacing are 0.04m × 0.04m. The simulated water surface profiles are shown in Fig.11(d). The phenomena is reasonably simulated by the model, as shown by the figure.

CONCLUSIONS

A second order accurate two-dimensional flood model is proposed. The effect of obstructions within a cell on the flow is treated as a drag force. The drag force term is modeled with a drag coefficient and an area ratio. The TVD-MacCormack scheme is employed for its high-resolution. The applicability and accuracy of the proposed model are tested against the Stoker's analytical solution and one- and two-dimensional dam-break problems in a horizontal channel with equi-spaced rigid cylinders. The

computed results agree well with both the analytical solution and the experimental data, indicating validity of the proposed numerical model. The effects of drag coefficient and area ratio on the flow are examined through numerical experiments. The model responses to these parameters are found to be reasonable. The work is continuing to include techniques for source term discretization and internal boundary conditions for flood simulation model.

ACKNOWLEDGEMENT

This research was supported by the Grant-in-Aid for Science Research for Ministry of Education and culture, Japan under Grant B(2), No.11450190. The authors wish to acknowledge the help of Dr. Akhilesh Kumar Jha and Mr. Takayuki Nukii.

REFERENCES

1. Iwasa, Y., Inoue, K. and Mizutori, M.: Hydraulic analysis of overland flood flows by means of numerical method, Annuals of the Disaster Prevention Research Institute, Kyoto University, Vol.23(B-2), pp.305–317, 1987, (in Japanese).
2. Takahashi, T. and Nakagawa, H.: Behavior of the over land flood flows in the Modeled urban area, Annuals of the Disaster Prevention Research Institute, Kyoto University, Vol.26B-2, pp.245–259, 1983, (in Japanese).
3. Suetugi, T. and Kuruki, M.: Research on Application for flood disaster prevention and simulation of flooding flow by means of new flood simulation model, Proceedings of the Hydraulic Engineering, JSCE, No.593/II-43, pp.41–50, 1998, (in Japanese).
4. Fukuoka, S., Kawashima, M., Yokoyama, H. and Mizuguchi, M.: The numerical simulation model of flood induced flows in urban residential area and the study of damage reduction, Proceedings of the Hydraulic Engineering, JSCE, No.600/II-43, pp.23–36, 1998, (in Japanese).
5. Fujii, K.: Numerical methods for computational fluid dynamics, University of Tokyo Press, pp.234, 1994, (in Japanese).
6. Xanthopoulos, T. and Koutitas, C.: Numerical simulation of a two-dimensional flood wave propagation due to dam failure, Journal of Hydraulic Research, Vol.14, No.4, pp.321–331, 1976.
7. Katopodes, N. and Strelkoff, T.: Computing two-dimensional dam-break flood waves, Journal of Hydraulic Engineering, ASCE, Vol.104, No.9, pp.1269–1288, 1978.
8. Glaister, P.: Approximate Riemann solution of the shallow water equations, Journal of Hydraulic Research, Vol.26, No.3, pp.293–306, 1988.
9. Alcrudo, F., Garcia-Navarro, P. and Saviron, J. M.: Flux difference splitting for 1-D open channel flow equations, International Journal for Numerical Methods in Fluids, Vol.14, pp.1009–1018, 1992.
10. Fraccarollo, L. and Toro, E. F.: Experimental and numerical assessment of the shallow water model for two-dimensional dam-break type problems, Journal of Hydraulic Research, Vol.33, No.6, pp.843–864, 1995.
11. Zhao, D. H., Shen, H. W., Lai, J. S. and Tabios III, G. Q.: Approximate Riemann solvers in FVM for 2D hydraulic shock wave modeling, Journal of Hydraulic Engineering, ASCE, Vol.122, No.12, pp.692–702, 1996.
12. Raupach, M. R. and Shaw, R. H.: Averaging procedures for flow within vegetation canopies, Boundary-Layer Meteorology, Vol.22, pp.79–90, 1982.
13. Ikeda, S., Kuga, T. and Chen, F.: Stability of organized horizontal vortices and momentum transport in open channel flows with bank vegetation, Proceedings of the Hydraulic Engineering, JSCE, No.551/II-37, pp.63–73, 1996, (in Japanese).
14. Akiyama, J., Ura, M., Yamaguchi, M. and Shigeeda, M.: Applicability of 2-D numerical model based on MacCormack scheme to shallow water flow, Annual Journal of Hydraulic Engineering, Vol.42, pp.679–684, 1998, (in Japanese).
15. Harten, A. and Hyman, J. M.: Self-adjusting grid method for one-dimensional hyperbolic conservation laws, Journal of Computational Physics, Vol.50, pp.235–269, 1983.
16. Sweby, P. K.: High resolution schemes using flux limiters for hyperbolic conservation laws, SIAM Journal of Numerical Analysis, Vol.21, No.5, pp.995–1011, 1984.
17. Stoker, J. J.: Water Waves, Interscience Publishers, Inc. Wiely and Sons, New York, pp.567, 1957.

APPENDIX - NOTATION

The following symbols are used in this paper:

a	=	coefficient of obstructions patterns (a =1:parallel, a = 2: staggered);
A	=	cell area;
A'	=	area within a cell circumscribing obstructions;
$\boldsymbol{A}$, $\boldsymbol{B}$	=	Jacobian of $\boldsymbol{E}$ and $\boldsymbol{F}$ with respect to $\boldsymbol{U}$, respectively;
c	=	wave speed($= \sqrt{gh}$);
C_d	=	drag forces coefficient;
C_r	=	Courant number;
d	=	projected width of a obstruction against main flow;
$\boldsymbol{E}$, $\boldsymbol{F}$	=	components of the flux;
F_x, F_y	=	drag forces along x and y directions;
g	=	acceleration due to gravity;
h	=	water depth;
h_r	=	reservoir depth;
h_t	=	tailwater depth;
I_x, I_y	=	obstructions spacing along x, y directions, respectively;
n	=	Manning's roughness coefficient;
S_{ox}, S_{oy}	=	bed-slopes along x and y directions, respectively;
S_{fx}, S_{fy}	=	friction slopes along x and y directions, respectively;
$\boldsymbol{S}_x$, $\boldsymbol{S}_y$	=	vectors containing source and sink terms.;
u, v	=	velocity components along x and y directions, respectively;
$\boldsymbol{U}$	=	vector of unknowns;
$\tilde{\alpha}$	=	wave strength;
Δt	=	time step;
Δx	=	grid size along x-direction;
θ_x	=	parameter determining the direction of space differences;
λ	=	area ratio;
λ'	=	density of obstructions in a cell for the considered patterns;
λ^k, e^k	=	eigenvalues and eigenvectors of $\boldsymbol{A}$;
ϕ	=	limiter;
Ψ	=	an entropy correction to $\tilde{\alpha}$; and
ω^k, f^k	=	eigenvalues and eigenvectors of $\boldsymbol{B}$.

(Received December 9, 1999 ; revised February 22, 2000)